

A NOVEL EXPERIMENTAL PROCEDURE TO DETERMINE THE COHESIVE LAW IN ENF TESTS.

A.Arrese¹, N. Insausti¹, F. Mujika¹

M. Perez-Galmés², J. Renart²

¹Materials+Technologies Group/ Mechanics of Materials, Faculty of Engineering of
Gipuzkoa (UPV/EHU), San Sebastián, Spain

²AMADE, Polytechnic School (II), University of Girona, Carrer Universitat de Girona, 4, E-
17003 Girona, Spain

Keywords: Interlaminar failure, Cohesive zone, ENF test, mode II

ABSTRACT

This study presents a novel method to determine the mode II cohesive law of unidirectional carbon fiber reinforced polymer laminates, employing the End Notched Flexure (ENF) test.

The fracture toughness in mode II (G) and crack shear displacement (Δ_t) are determined based on a compliance variation data reduction method (BTBR) by processing the global load displacement curve, without monitoring the crack length and the crack shear displacement during the test. The procedure is validated by finite element analysis including cohesive zone modeling. The results of the method are compared to those obtained with the Direct Method, where the fracture toughness is determined based on the rotations of the load introduction points and the crack shear displacement is directly measured. It is concluded that the proposed data reduction scheme is suitable to obtain the mode II cohesive law using only the load and displacement data obtained from the testing machine, without any external displacement measurement technique and without any assumption of the form of the cohesive law.

1. INTRODUCTION

Delamination is a particularly dangerous damage mode of composite materials. Interlaminar cracks, which can initiate at a free edge or at defects from manufacturing, are very difficult to detect and their presence may significantly reduce the global stiffness and compressive strength of the structure. Thus, modeling of the interlaminar behavior is crucial for safe design of an advanced structural component.

With respect to interlaminar failure in mode II, the End-Notched Flexure (ENF) test, the End-Loaded Split (ELS) test and the Four-Point End-Notched Flexure (4ENF) test are the most popular test adopted in literature. The ENF test and the ELS test have been recently standardized as ASTM D7905 [1] and ISO 15114 [2], respectively.

These test configurations have some advantages and disadvantages. The ENF is the most used test due to its simple fixture but the specimen dimensions should be selected accurately in order to avoid unstable crack initiation [3,4]. The 4ENF test provides stable crack propagation, but the measured critical energy release rate, G_{IIc} , is dependent on specimen geometry and it is affected by friction [5, 6]. The ELS test provides stable crack initiation, but the results are affected by the clamp end of specimen and large displacement [7, 8, 9]. Therefore, in the present study, ENF configuration is adopted.

Finite element method is widely used to simulate initiation and propagation of delamination in composite structures. Among the available methods for the investigation of crack propagation by means of finite element codes, the Virtual Crack Closure Technique (VCCT) or its alternative two-step extension procedure (TSEP) and the cohesive zone model (CZM) are extensively used [10 - 17].

VCCT formulated by Rybicki and Kanninen [18] and TSEP proposed by Bonhomme et al. [19] are computationally simple and they are considered effective methods for determining the energy release rate. Nevertheless, they are not suitable analyzing the delamination growth.

CZM was introduced in the early sixties by Barenblatt [20] and Dugdale [21] and describes the local fracture processes near the crack tips as a gradual phenomenon where the separation takes place across a cohesive zone. It is widely used in the commercial finite element packages due to the applicability for analyzing the fracture of different materials under different load conditions.

With CZM, fracture is modeled as a process where a surface in the material first forms a cohesive zone called the fracture process zone (FPZ). The FPZ is later separated into two crack surfaces. In the cohesive zone, the crack surfaces are held together by cohesive tractions.

The general idea is that the fracture process is described by a local stress-relative displacement relation of a fracture process zone (FPZ). This relation is a constitutive law of the material, named cohesive law. The fracture process zone length (L_{FPZ}) is the distance at the crack plane where the cohesive tractions are acting. Fig. 1 illustrates a cohesive model, where after damage initiation, the traction is assumed to decrease as the relative displacement of the cohesive surfaces increases. For a critical displacement, the traction is zero and a new crack surface is created.

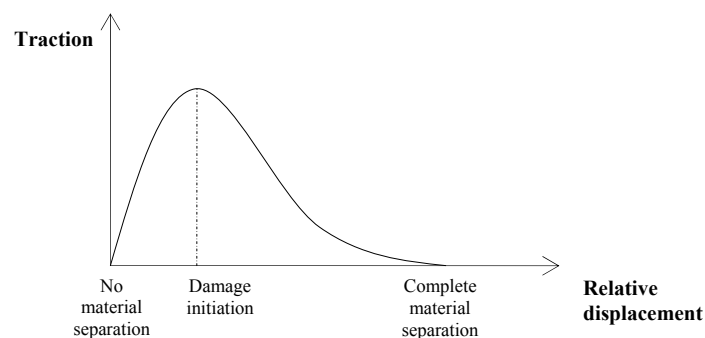


Fig.1. General Form of a cohesive zone law

It is shown that the shape of the cohesive law plays an important role in the simulation of the fracture behavior of materials [22]. Thus different methods to determine the cohesive law of adhesive layers and laminated composites have been developed [23 -39].

In order to determine relative displacements at the crack tip, the use of external equipment as Digital Image Correlation (DIC), Linear voltage differential transformer (LVDT) or Crack Tip Opening Displacement sensor (COD) are required [24,25,27-3839]. Experimental difficulties related to inaccurate results in the measurement of very small crack tip separations have been reported, [25, 33].

In the present study, a new method to determine the cohesive law in Mode II has been developed similar to the one recently presented for Mode I [40]. It is based on the determination of the **equivalent crack** length due to the compliance variation of the specimen **as the FPZ develops**, for every pair of load and displacement data recorded during the test. This method, named Beam Theory with Bending Rotations (*BTBR*) includes geometrical nonlinearities and shear and local deformations effects [41]. Therefore, the energy release rate as a function of the **equivalent crack** advance is determined using only the load and displacement data obtained from the testing machine. Based on the same analytic approach, the crack tip shear displacement, Δ_t , is determined as a function of the equivalent crack advance **at the initial crack tip position that corresponds to the insert length**. Therefore, G can be expressed as a function of Δ_t and the cohesive law is obtained by numerical differentiation of G with respect to Δ_t . The BTBR procedure is compared with the Direct Method (DM), where the fracture toughness is determined based on the rotations of the load introduction points **avoiding the need of monitoring the crack length during the test** and the crack shear displacement is directly measured **at the initial crack tip position**. In order to analyze if the proposed data reduction scheme is suitable for assessing the Cohesive laws in Mode II, Finite Element simulations of the ENF test including cohesive zone modeling have been carried out in ABAQUS and the accuracy of the obtained Cohesive laws have been discussed.

2. ANALYTIC APPROACH

2.1. Cohesive zone model

The path independent J -integral, presented by Rice [42] can be used to calculate the fracture resistance J during the crack growth.

$$J = \int_C \left(W dy - \mathbf{T} \frac{\partial \mathbf{u}}{\partial x} dC \right) \quad (1)$$

Where C is the counter clockwise integration path, W is the strain energy density, \mathbf{T} the traction vector and \mathbf{u} the displacement vector. By choosing C close to the crack tip, \mathbf{T} is null [23] and Eq. (1) becomes in:

$$J = \int_C W dy = \int_0^{\Delta_n} \sigma d\Delta_n + \int_0^{\Delta_t} \tau d\Delta_t \quad (2)$$

where σ , τ , Δ_n and Δ_t are the cohesive normal stress, shear stress, opening and shear displacement at the crack tip, respectively.

According to Eq. (2) if the relationship among J , Δ_n and Δ_t is known, the cohesive laws can be obtained as

$$\sigma(\Delta_n, \Delta_t) = \frac{\partial J}{\partial \Delta_n} \quad \tau(\Delta_n, \Delta_t) = \frac{\partial J}{\partial \Delta_t} \quad (3)$$

Furthermore it is shown that the J -integral is equivalent to Energy Release Rate G for an elastic material [43,44].

Being Π the potential energy in an elastic body $\Pi = U - F_i \delta_i$ and U^* the complementary strain energy stored in the body $U^* = F_i \delta_i - U$. It results that

$$U^* = -\Pi \quad (4)$$

Then

$$J = -\frac{1}{w} \frac{d\Pi}{da} = \frac{1}{w} \left(\frac{\partial U^*}{\partial a} \right)_{F_i} = G \quad (5)$$

where a is the crack length, w is the width and the subscript F_i follows the partial derivative convention indicating the load variable is held constant during partial differentiation.

For a symmetric specimen, loaded in three point bending with a crack advancing along the mid-plane, the crack tip shear displacement is tangential to the crack plane and the crack tip normal displacement is zero. Then, the cohesive shear stress τ depends only on the shear Δ_t [44], being

$$\tau(\Delta_t) = \frac{\partial G}{\partial \Delta_t} \quad \text{or} \quad \tau(\Delta_t) = \frac{\partial J}{\partial \Delta_t} \quad (6)$$

2.2. Determination of the Fracture toughness.

2.2.1 *J* Integral method

The path independent *J* integral can be applied for characterizing the fracture process zone under the assumption of bulk elastic behavior, small strain and small displacement and no body forces [30, 44]. The *J* integral can be applied choosing the integral path locally along the crack faces enclosing the cohesive zone and crack tip $\Gamma_{loc} = \Gamma_1 + \Gamma_{tip} + \Gamma_2$, as shown in Fig 2. The *J* integral results:

$$J_{loc} = J_{tip} + \int_0^{\Delta_n} \sigma d\Delta_n + \int_0^{\Delta_t} \tau d\Delta_t \quad (7)$$

where J_{tip} is the *J* integral around the crack tip.

On the other hand, if *J* integral is applied choosing the integral path along the external boundaries of the fracture specimen as shown in Fig. 2, and due to path independence of the *J* integral, it can be written as:

$$J_{ext} = J_{loc} = J_{tip} + \int_0^{\Delta_n} \sigma d\Delta_n + \int_0^{\Delta_t} \tau d\Delta_t \quad (8)$$

During loading the specimen, crack initiation occurs when J_{tip} is equal to the initiation fracture energy J_0 . With increasing loading, the damage is assumed to grow with J_{tip} being equal to J_0 . With increasing damage length, the cohesive zone develops. The cohesive zone length and the crack tip relative displacement increases as the damage extends, and thus the energy uptake of cohesive zone increases in accordance with Eq 8. The fracture resistance *J* increases as the damage propagates and when Δ reaches the value for which the cohesive stress vanishes Δ_c the *R*-curve attains a steady state value J_c .

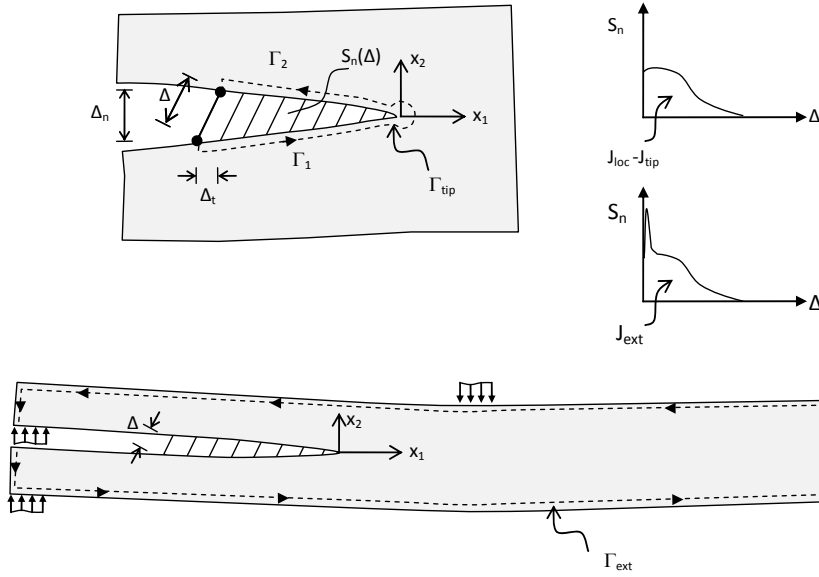


Fig. 2. Integration path for the J integral: a) integration path locally around the cohesive zone, b) interpretation of traction vs. separation in FPZ, and c) Integration path along external boundaries of ENF test

The value of $J = J_{ext} = J_{loc}$ during the fracture process is denoted J , the fracture resistance of the material.

$$J = J_0 + \int_0^{\Delta_n} \sigma d\Delta_n + \int_0^{\Delta_t} \tau d\Delta_t \quad (9)$$

The J -integral closed-form solution for the ENF test proposed by Stigh et al. [36] was used for computing J as:

$$J = \frac{P}{2w} [\theta_A - 2\theta_C + \theta_B] \quad (10)$$

where w is the specimen width, P is the applied load and θ_A , θ_B and θ_C are the clockwise rotation at the load introduction points as it is shown in Fig. 3.

2.2.2 Beam theory with bending rotation (BTBR) method

The end notched flexure (ENF) test configuration is shown in Fig. 3 [41]. It is assumed elastic behavior of the adherents during the entire fracture test process. In order to achieve pure mode II, a pre-cracked specimen is loaded at three point flexure fixture.

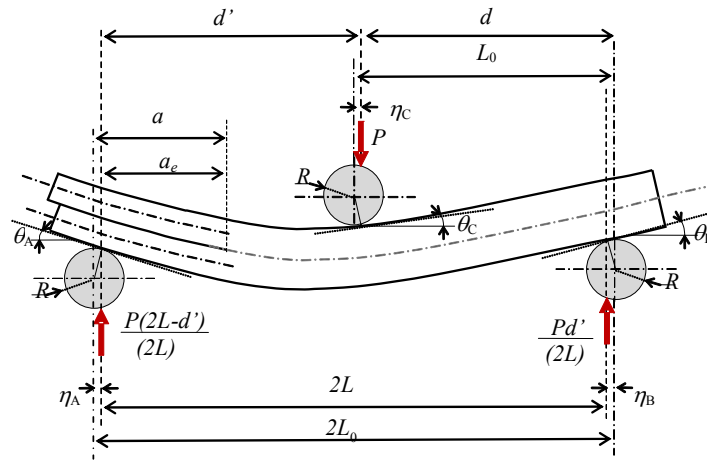


Fig. 3: Schematic ENF specimen according to BTBR [41]

The first step of the presented analyses is to evaluate the mode II fracture energy release rate G_{II} . For this purpose, a method proposed by Arrese et al [41] is used. The energy release rate is determined without any optical measurement of the crack length, taking into account the bending rotation effects, shear effects and local deformation effects. The **equivalent crack** length is obtained based on the compliance after having determined the elastic properties of the specimen [45]. In this way, the **equivalent crack** length is defined at each point of the test data, and thus a continuous plot of the R -curve can be also determined.

The displacement of the loading point is determined applying the Engesser–Castigliano’s theorem [17,46], which in the case of shear and bending is given by

$$\delta_i = \left[\frac{\partial U^*}{\partial F_i} \right]_a = \int_L \frac{M}{E_f I} \frac{\partial M}{\partial F_i} dx + \int_L \frac{6}{5} \frac{Q}{G_{13} A} \frac{\partial Q}{\partial F_i} dx \quad (11)$$

Being F_i an independent applied force; δ_i the displacement of the application point of F_i in the direction of F_i ; M is the bending moment; Q is the shear force; E_f is the flexural modulus; G_{13} is out-of-plane shear modulus; I is the second moment of area; A is the cross sectional area.

The derivatives of bending moments and shear forces are obtained applying a vertical unit load at the middle point of the specimen. The middle point displacement is:

$$\delta = \frac{P}{8E_f wh^3} \left(3(a)^3 [1 - 3\alpha_a] + 2L_0^3 \right) [1 - \alpha_f] + \frac{3PL_0}{10G_{13}wh} [1 - \alpha_s] \quad (12)$$

Where

$$\begin{aligned} \alpha_a &= \frac{R\varepsilon}{(2h)} \frac{(-a_0^3 + 3a_0^2 + 1)}{a_0} \\ \alpha_f &= \frac{3R\varepsilon}{(2h)} \frac{(4a_0^6 - 3a_0^5 + 3a_0^2 + 2)}{(2 + 3a_0^3)} \\ \alpha_s &= \frac{R\varepsilon}{(2h)} \frac{(3a_0^2 + 2)}{2} \end{aligned} \quad (13)$$

Being $2h$ the thickness, w the width, $\varepsilon = \frac{3P(2L_0)}{2E_f w(2h)^2}$ and $a_0 = \frac{a}{L_0}$

Taking into account Eq. (12), the compliance of ENF specimen can be written as:

$$C = \frac{\delta}{P} = \frac{1}{8E_f wh^3} \left(3(a)^3 [1 - 3\alpha_a] + 2L_0^3 \right) [1 - \alpha_f] + \frac{3L_0}{10G_{13}wh} [1 - \alpha_s] \quad (14)$$

In order to determine the **equivalent crack** length, Eq. (14) is equated to the experimental value computed directly from the measured load–displacement curve, corrected with the system compliance. This procedure leads to obtain the **equivalent crack** length at any point of the test where P and δ are evaluated. Taking into account that $U^* = \int \delta dP$ According to Eq. (5) and Eq. (12), G is:

$$\begin{aligned} G &= \frac{9Pa^2}{2E_f w^2 (2h)^2} [1 - \chi] \\ \chi &= \frac{2R}{(2h)} \varepsilon \left[\frac{8}{3} a_0^3 - \frac{25}{6} a_0^2 + 6a_0 + \frac{1}{9a_0} \left(15 + \frac{12}{5} \frac{E_f}{G_{13}} \left(\frac{h}{L_0} \right)^2 \right) \right] \end{aligned} \quad (15)$$

2.3. Crack Tip Shear Displacement

In the current approach the Fracture Process Zone (FPZ) development is assumed to be analogous to an equivalent crack advance Δa , related to the compliance variation. Indeed, the development of the FPZ is related to an increase of the compliance that in the current approach is associated to an equivalent crack advance.

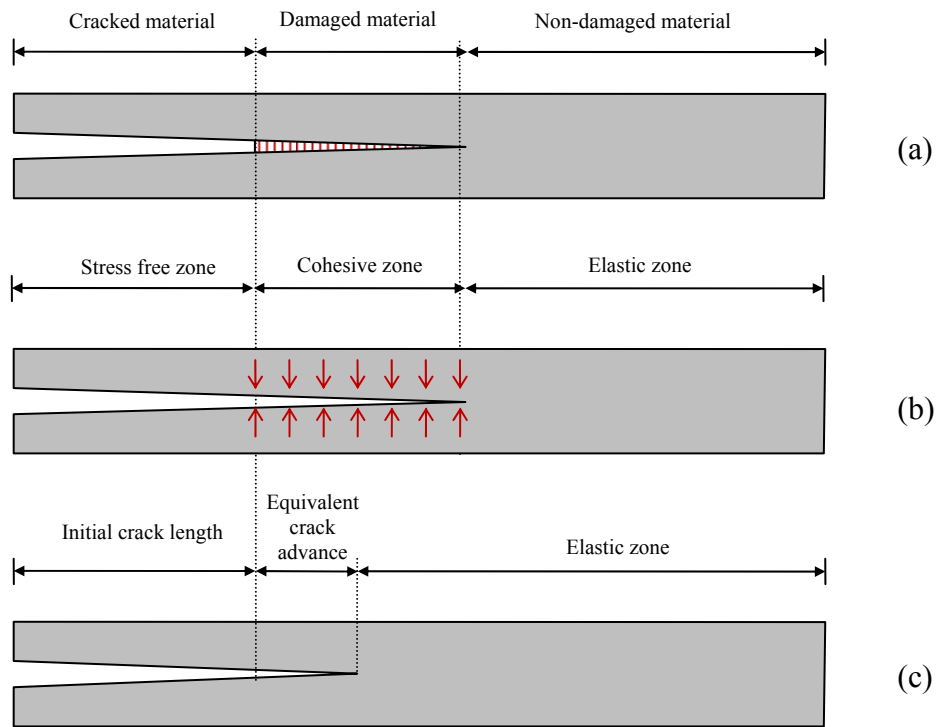


Fig. 4: FPZ of a quasi brittle material (a), Cohesive zone model concept (b) and the Equivalent approach proposed in the present work (c).

Fig. 4 (a) shows the real system where the material is cracked in one end, followed by the damage zone and finally the non-damaged material. Fig 4 (b) shows the system according to CZM where the damage zone is represented by a cohesive zone where the crack surfaces are held together by cohesive tractions. Fig. 4 (c) shows the equivalent crack length system, which is the basic assumption of the current proposal, where the effect of the damage zone development in the behavior of the system is represented by an equivalent crack advance.

Then, the crack tip shear displacement Δ_t at the initial crack tip position is obtained according to the assumption of the system based on the equivalent crack length as shown in Fig 5.

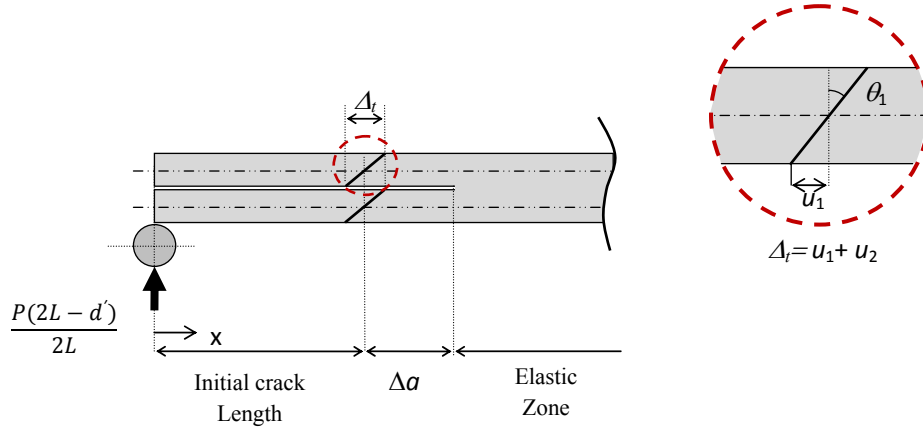


Fig. 5: Initial crack tip shear displacement

The unit load method and the Engesser–Castigliano’s theorem given in Eq. (11) are used applying two opposite unit loads at the initial crack tip position in order to get the derivatives of bending moment and shear force. The relative shear displacement at the initial crack tip is given by:

$$\Delta_t = u_2 + u_1 = \frac{3}{E_f w h^2} \frac{P(2L - d')}{2L} [a^2 - a_{ie}^2] \quad (16)$$

Where

$$\begin{aligned} 2L &= 2L_0 \left[1 - \frac{R}{2L_0} (|\theta_A| + |\theta_B|) \right] \\ d' &= L_0 \left[1 - \frac{R}{L_0} (|\theta_A| - |\theta_C|) \right] \\ a_{ie} &= a_i \left[1 - \frac{R}{a_i} |\theta_A| \right] \\ a_e &= a \left[1 - \frac{R}{a_i} |\theta_A| \right] \end{aligned} \quad (17)$$

where a_i is the initial crack length and a is the **equivalent crack** length determined during the test.

Replacing the corrected parameters of Eq. (17) in Eq. (16), the following equation is obtained:

$$\Delta_t = u_2 + u_1 = \frac{6P}{4E_f w h^2} [a_e^2 - a_{ie}^2] [1 - \psi] \quad (18)$$

Where

$$\psi = R \left[-\frac{|\theta_A|}{2L_0} + \frac{|\theta_B|}{2L_0} + \frac{|\theta_C|}{L_0} \right] \quad (19)$$

$|\theta_A|$, $|\theta_B|$ and $|\theta_c|$ are obtained from the analysis carried out in [47].

3. NUMERICAL VERIFICATION OF THE PROPOSED METHOD

A finite element analysis of the ENF specimen was used to assess the accuracy of the proposed method compared with the Direct Method. In the considered ENF specimen configuration the specimen length is $2L = 120$ mm; the width is $w = 25$ mm and the arm thickness is $h = 2$ mm; the elastic properties corresponding to the specimen that are shown on table 1 are typical values of unidirectional carbon epoxy composite laminated materials used in aeronautical industry.

E_{11} (GPa)	$E_{22}=E_{33}$ (GPa)	$G_{12}=G_{13}$ (GPa)	G_{23} (GPa)	$\nu_{12}=\nu_{13}$	ν_{23}
120.0	7.8	4.0	2.8	0.34	0.4

Table 1. The material mechanical properties

The model was developed in ABAQUS [48] using four-node 2D plane strain elements (CPE4) (Fig. 6). A row of zero-thickness four-node cohesive elements (COH2D4) was placed ahead of the notch tip to model crack propagation. The following input cohesive laws have been used to represent a thin interface with a medium toughness.

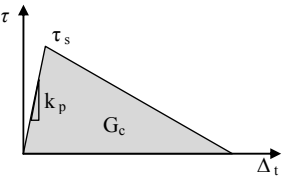
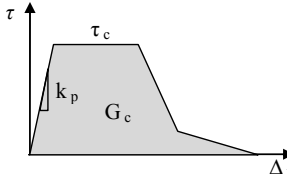
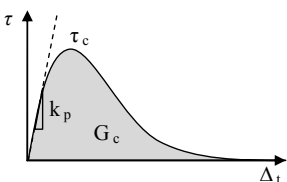
Bilinear			Tabular with a Bilinear Softening			Exponential			
G_c [N/mm]	τ_s [MPa]	K_p [N/mm ³]	G_c [N/mm]	τ_s [MPa]	K_p [N/mm ³]	G_c [N/mm]	τ_s [MPa]	K_p [N/mm ³]	α
5	50	10^6	5	70,50,30	10^6	5	50	10^6	2,5,-5
									

Table 2. Cohesive laws used in the finite element analyses.

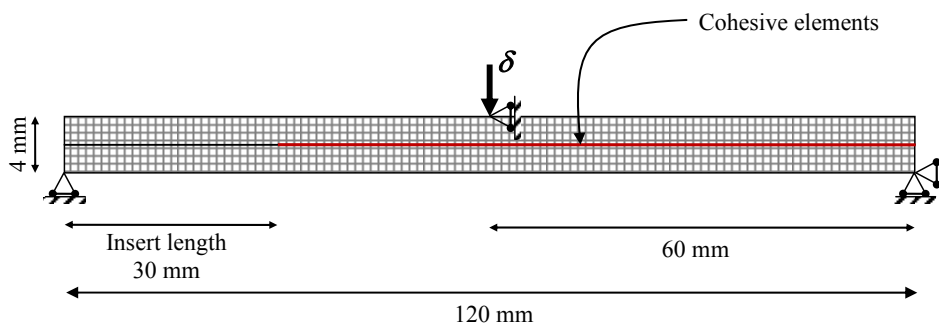


Fig. 6 Finite Element model (dimensions and boundary conditions)

As the support rollers have not been included in the model, then $R = 0$ mm has been assumed in the BTBR method.

The aim of this numerical validation is to check if the cohesive law used in the model input can be determined based on the data reduction method proposed in the present work. Two different procedures are used in order to get the input cohesive law.

- 1) **Direct method (DM):** According to the first procedure, the methodology used by several authors [24, 25, 27 -36] to determine experimentally the cohesive law is reproduced virtual test. J is computed replacing in Eq. (10) rotations at the support and the loading application point. The relative displacement corresponds to a pair of homologous points on the cohesive line located at the initial crack tip. Finally, the cohesive law is obtained by numerical differentiation.
- 2) **BTBR:** The load-displacement data are recorded and G and Δ_t are determined from Eqs. (14) and (16), respectively. Finally, the cohesive law is obtained by numerical differentiation.

4. RESULTS AND DISCUSSION

In order to validate the proposed data reduction scheme, the BTBR and DM have been applied to determine the fracture toughness from numerical results.

The corresponding Load vs load point displacement curve for the bilinear cohesive law is shown in Fig.7.

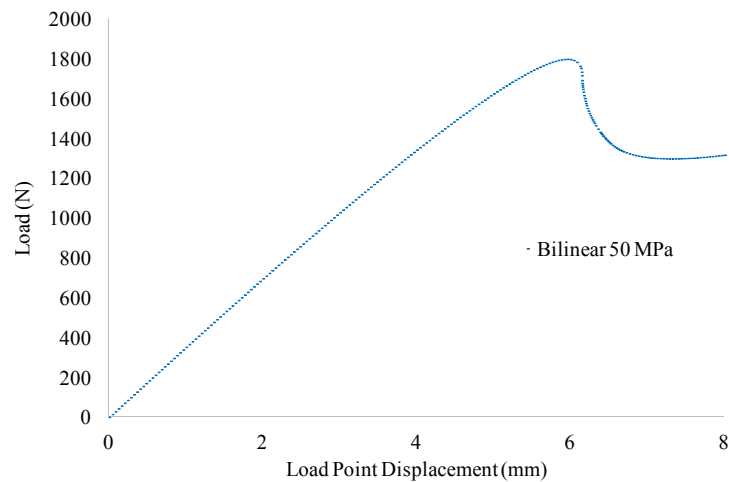


Fig. 7 Load vs. Load Point Displacement for the bilinear CL

The corresponding G and J vs load point displacement curves for the bilinear cohesive law are shown in Fig.8.

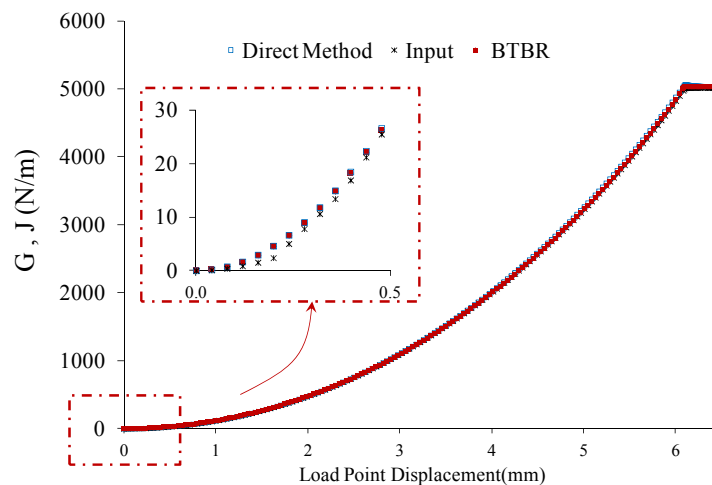


Fig. 8 Interlaminar Toughness vs. Load Point Displacement for the bilinear CL

In Fig. 9, Δ_t determined by FEM at the initial notch tip, and Δ_t obtained by the proposed data reduction method corresponding to the bilinear cohesive laws are plotted.

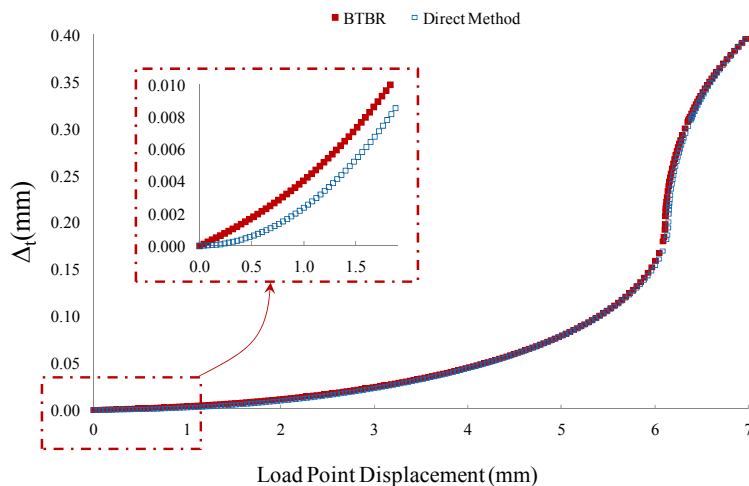


Fig. 9 Crack tip shear displacement vs. Load Point Displacement for the bilinear CL

Fig. 10 shows the fracture toughness versus crack tip shear displacement curves corresponding to the bilinear cohesive laws. The J - Δ_t curves according to the DM in blue, G - Δ_t curves according to BTBR in red and the input data in black.

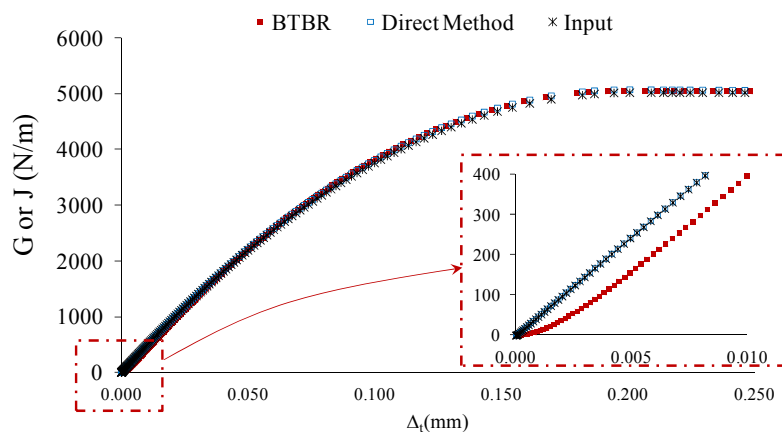


Fig. 10. Interlaminar Toughness vs. Crack tip shear displacement for the bilinear CL

Fig. 11 shows a comparison among the input cohesive law and those obtained by numerical differentiation of the curves shown in Fig. 10 with respect to Δ_t .

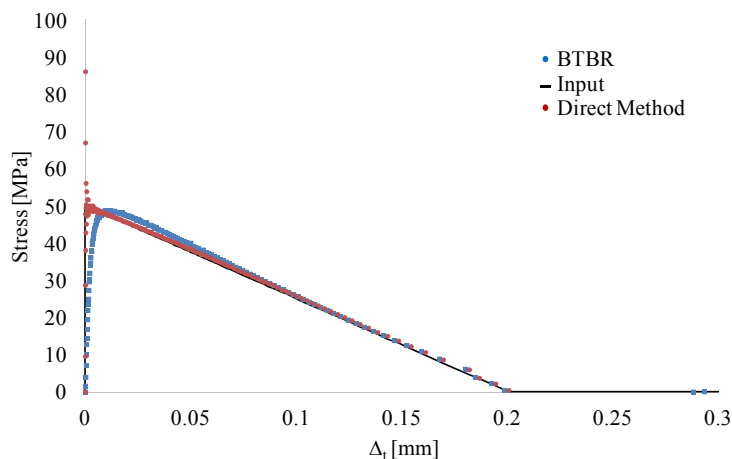


Fig. 11: Cohesive law bilinear CL $\tau_s=50\text{MPa}$; $G=5\text{N/mm}$; $K_p=10^6\text{ N/mm}^3$

In order to check the suitability of the proposed method to determine different cohesive laws, interfaces with tabular and exponential constitutive laws listed in Table 2 are simulated. The corresponding Load vs Load point displacement curves are shown in Fig.12 and the results are shown in Fig. 13.

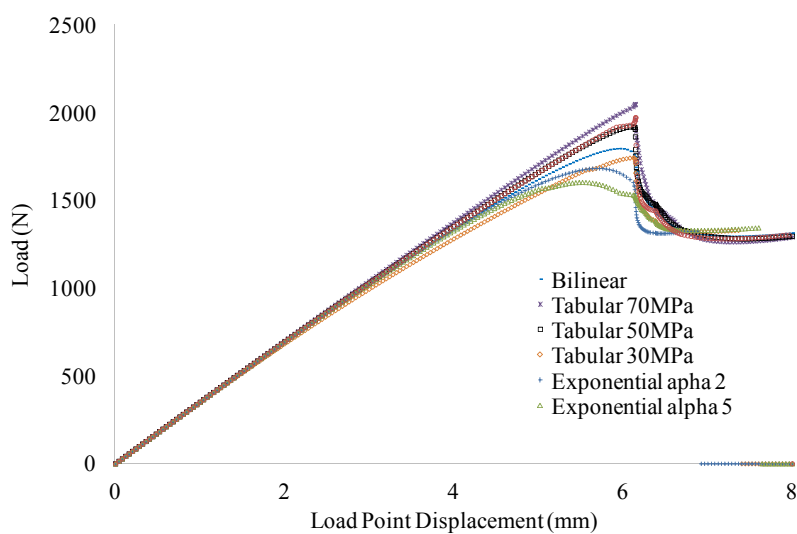


Fig. 12: Load vs. Load Point Displacement for all simulated CLs

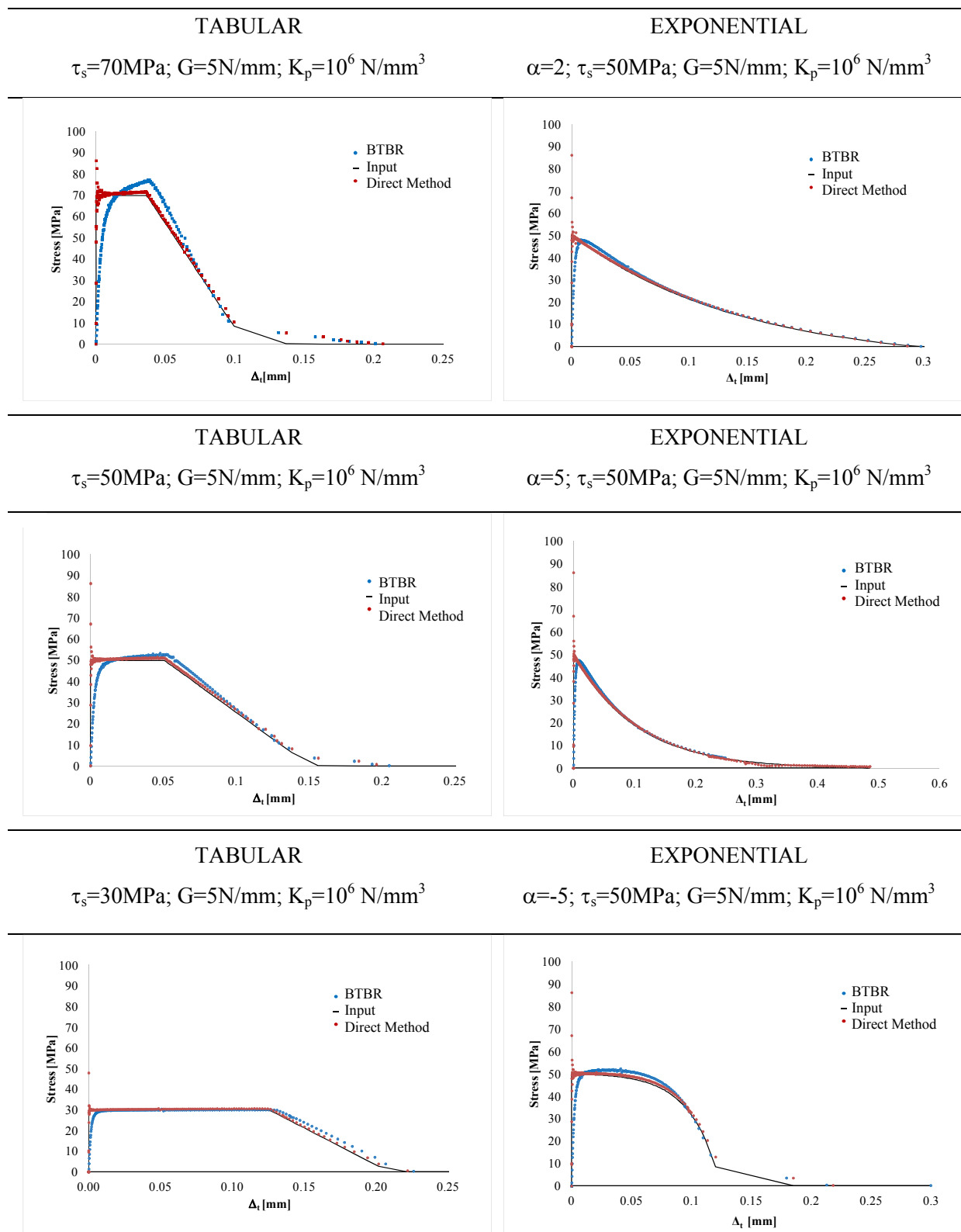


Fig. 13: Results of the Tabular and Exponential CL listed in Table 2.

According to Fig. 11 and Fig. 13, it can be seen that in general features, a good prediction of the input cohesive law is obtained with both methods. It is observed that the results obtained from the DM and BTBR methods are generally well correlated. As it is shown in Fig. 11 and Fig. 13 the proposed method BTBR is able to predict the shape and the maximum stress of each input cohesive law. An excellent agreement has been obtained in the softening region characterizing the fracture process but the initial part of the cohesive law, the penalty stiffness, reveals a discrepancy with respect to the input law, which may be originated by both numerical and precision problems.

In order to evaluate the accuracy of the results, predicted maximum shear stresses and the difference with respect the reference values are shown in Table 3. In order to establish the maximum stress for the DM data reduction scheme, the initial values are neglected. For the bilinear cohesive law, data $\Delta_t < 1\mu\text{m}$ are not considered. For the rest of the cases data correspond to $\Delta_t > 5\mu\text{m}$.

		Maximum Stress (MPa)				
		Input value	BTBR value	$\psi_{BTBR}(\%)$	DM. value	$\psi_{J int}(\%)$
Bilinear		50	48.8	2.4	51.8	3.6
		70	77.2	10.3	70.9	1.4
Tabular		50	53.1	6.2	49.6	0.8
		30	30.4	1.3	29.9	0.3
Exponential	$\alpha=2$	50	48.1	3.8	51.6	3.2
	$\alpha=5$	50	47.6	4.8	51.6	3.2
	$\alpha=-5$	50	52.3	4.6	51.9	3.8

$$\psi_{BTBR}(\%) = \frac{\tau_{S input} - \tau_{S BTBR}}{\tau_{S input}} \cdot 100 \quad \psi_{J int}(\%) = \frac{\tau_{S input} - \tau_{S DM}}{\tau_{S input}} \cdot 100$$

Table 3. Maximum shear stresses.

The critical interlaminar toughness determined with DM and BTBR approach and the difference with respect the reference values are shown in Table 4.

In order to evaluate the accuracy of the determined cohesive laws the area under the cohesive law is compared with the reference value used in FEA. The $G - \Delta_t$ curves are truncated at the test point where the load drops suddenly. As it can be seen in Table 4, there is a good agreement on the interlaminar toughness values obtained by both methods.

		Interlaminar Toughness (N/mm)				
		Input value	BTBR value	$\chi_{BTBR}(\%)$	DM. value	$\chi_{DM}(\%)$
Bilinear		5	5.12	2.4	5.15	3.0
	$\tau = 70\text{MPa}$	5	5.02	0.4	5.08	1.6
Tabular	$\tau = 50\text{MPa}$	5	5.07	1.4	5.04	0.8
	$\tau = 30\text{MPa}$	5	5.12	2.4	5.00	0.0
Exponential	$\alpha = 2$	5	5.13	2.6	5.16	3.2
	$\alpha = 5$	5	4.99	0.2	5.01	0.2
	$\alpha = -5$	5	4.94	1.2	4.95	1.0

$$\chi_{BTBR}(\%) = \frac{G_{C \text{ input}} - G_{C \text{ BTBR}}}{G_{C \text{ input}}} \cdot 100 \quad \chi_{DM}(\%) = \frac{G_{C \text{ input}} - G_{C \text{ DM}}}{G_{C \text{ input}}} \cdot 100$$

Table 4. Critical interlaminar toughness.

Finally with regard to the initial part of the cohesive laws, in Fig. 11 and Fig. 13 it can be seen that the prediction of the initial part of the CLs by the DM is slightly better than the one predicted by BTBR. The error in the prediction of the penalty stiffness by both methods shows that there is an initial discrepancy between local and global behavior, presumably originated by the fact that both approaches consider the system transversely infinitely rigid and also due to FE simulation inherent errors.

The difference in the local and global behavior causes the slight errors with respect the input values in J at the initial part of the test shown in Fig. 8 and are source of the errors in the

penalty stiffness and the oscillation at the initial values of the cohesive law predicted by DM in Figs 11, 13.

In the case of the BTBR, in addition to the discrepancy between local and global behavior, that affects not only the determination of G but also the determination of Δ_t , the error due to the equivalent crack advance system approach should also be considered as source of the error in the penalty stiffness of the predicted law.

In Fig 9 it can be seen that the error in the determination of Δ_t is more pronounced at the initial part of the test where the length of the developed FPZ and therefore the equivalent crack advance is small.

5. SUMMARY AND CONCLUSIONS

In the present paper, a new method for the determination of mode II cohesive law for unidirectional composite is proposed. The approach is based on the correlation between the developed Energy Release Rate (G) as a function of crack tip shear displacement (Δ_t). The Resistance Curves are determined obtaining the G as a function of the equivalent crack advance based on the compliance variation of the specimen as crack advances. The crack tip shear displacement is determined as a function of the equivalent crack advance assuming that the Fracture Process Zone development is analogous to an equivalent crack advance, related to the compliance variation. These measurements are used to compute the Energy Release Rate and crack shear displacement. The experimental cohesive law is determined by numerical differentiation.

The suitability of the method and the accuracy of the predicted cohesive laws have been demonstrated numerically by using Finite Element simulation of the ENF test including different cohesive zone models. The results obtained reveal that the proposed method is able to predict the shape, the maximum stress and toughness of each input cohesive law. An excellent agreement has been obtained in the softening region but discrepancies with respect

to the input law at the penalty stiffness have been detected originated by both numerical and precision problems.

It can be concluded that the proposed method provides a simple way to approach the mode II cohesive law using only load-displacement data provided by the universal testing machine, without the need of any external displacement measurement and without assuming the shape of the cohesive law.

ACKNOWLEDGMENTS

This work has been partially funded by the Spanish Government (Ministerio de Economía y Competitividad) under contract TRA2015-71491-R. Financial support of the University of the Basque Country (UPV/EHU) in the Research Group GIU 16/51 “Mechanics of Materials” is acknowledged.

REFERENCES

- [1] ASTM D7905, Standard Test Method for Determination of the Mode II Interlaminar Fracture Toughness of Unidirectional Fiber-Reinforced Polymer Matrix Composites, 2014.
- [2] ISO 15114, Determination of the mode II fracture resistance for unidirectionally reinforced materials using the calibrated end-loaded split (C-ELS) test and an effective crack length approach, 2014.
- [3] P. Davies, G.D. Sims, B.R.K. Blackman, A.J. Brunner, K. Kageyama, M. Hojo, K. Tanaka, G. Murri, C. Rousseau, B. Gieseke, R.H. Martin, Comparison of test configurations for the determination of unidirectional carbon/epoxy composites, an international round robin, *Plast. Rubber Compos.* 28 (1999) 432–437.
- [4] A.J. Brunner, B.R.K. Blackman, P. Davies, A status report on delamination resistance testing of polymer-matrix composites, *Eng. Fract. Mech.* 75 (2008) 2779–2794.
- [5] R. Martin, B.D. Davidson, Mode II fracture toughness evaluation using a four point bend end notched flexure test, in: *Proceedings of the 4th International Conference on Deformation and Fracture of Composites*, Institute of Materials, 1997.
- [6] P. Davies, Summary of Results From the Second VAMAS Mode II Round Robin Test Exercise Using the 4ENF Specimen. IFREMER Report TMSI/RED/MS, July 1999.
- [7] H. Wang, T. Vu-Khanh, V.N. Le, Effects of large deflection on mode II fracture test of composite materials, *J. Compos. Mater.* 29 (1995) 833–849.
- [8] D.R. Moore, A. Pavan, J.G. Williams, *Fracture mechanics testing methods for polymers, adhesives and composites*ESIS Publication 28, Elsevier Science Ltd, 2001.
- [9] M. Pérez-Galmés, J. Renart, C. Sarrado, A. Rodríguez-Bellido, J. Costa. A data reduction method based on the J-integral to obtain the interlaminar fracture toughness in a mode II end-loaded split (ELS) test. *Composites Part A: Applied Science and Manufacturing* 90 (2016) 670-677
- [10] S. Hashemi, A.J. Kinloch, J.G. Williams. Corrections needed in double-cantilever beam tests for assessing the interlaminar failure of fibre-composites. *J Mater Sci Lett* 8 (1989) 125–29.
- [11] H. Yoshihara, T. Kawamura. Mode I fracture toughness estimation of wood by DCB test. *Compos Part A* 37 (2006) 2105–13.
- [12] MFSF. De Moura, J.L. Morais, N. Dourado. A new data reduction scheme for mode I wood fracture characterization using the double cantilever beam test. *Eng Fract Mech* 75 (2008) 3852–65.

-
- [13] MFSF. De Moura, RDSG. Campilho, JPM. Gonçalves. Crack Equivalent concept applied to the fracture characterization of bonded joints under pure mode I loading. *Compos Sci Technol* 68 (2008) 2224–30.
- [14] MFSF. De Moura, RDSG. Campilho, AM. Amaro, PNB. Reis. Interlaminar and intralaminar fracture characterization of composites. *Compos Struct* 92 (2010) 144–9.
- [15] JLL. Morais, MFSF. De Moura, FAM. Pereira, J. Xavier, N. Dourado, MIR. Dias. The double cantilever beam test applied to mode I fracture characterization of cortical bone tissue. *J Mech Behavior Biomed Mater* 3 (2010) 446–53.
- [16] V. Mollón, J. Bonhomme, J. Viña, A. Argüelles. Theoretical and experimental analysis of carbon epoxy asymmetric dcb specimens to characterize mixed mode fracture toughness. *Polym Test* 29 (2010) 766-770.
- [17] A. Boyano, V. Mollón, J. Bonhomme, J. De Gracia, A. Arrese, F. Mujika. Analytical and numerical approach of an End Notched Flexure test configuration with an inserted roller for promoting mixed mode I/II. *Eng Fract Mech* 143 (2015) 63–79.
- [18] EF. Rybicki, MF. Kanninen. A finite element calculation of stress intensity factors by a modified crack closure integral. *Eng Fract Mech* 9 (1977) 931–8.
- [19] J. Bonhomme, A. Argüelles, MA. Castrillo, J. Viña. Computational models for mode I composite fracture failure: the virtual crack closure technique versus the two-step extension method. *Meccanica*. 45 (2010) 297-304.
- [20] GI. Barenblatt. Mathematical Theory of Equilibrium Cracks in Brittle Fracture. *Adv Appl Mech*. 7 (1962) 55-129.
- [21] DS. Dugdale. Yielding of steel sheets containing slits. *Mech. Phys. Solids* 8 (1960) 100–104.
- [22] C. Shet, N. Chandra, Effect of the shape of Tcd cohesive zone curves on the fracture response, *Mech. Adv. Mater Struc* 11 (2004) 249-275.
- [23] JL. Hogberg, BF. Sørensen, U. Stigh. Constitutive behaviour of mixed mode loaded adhesive layer. *Inter J Sol Struct*. 44 (2007) 8335–54.
- [24] K. Leffler, KS. Alfredsson, U. Stigh. Shear behaviour of adhesive layers. *Int. J. Sol Str* 44 (2007) 530- 45.
- [25] C. Sarrado, A. Turon, J. Costa, J. Renart. An experimental analysis of the fracture behavior of composite bonded joints in terms of cohesive laws. *Compos Part A*. 90 (2016) 234–42.
- [26] A. Soto, E. González, P. Maimí, A. Turon, JR. Sainz de Aja, FM. de la Escalera. Cohesive zone length of orthotropic materials undergoing delamination. *Eng Fract Mech*. 159 (2016) 174– 88.

-
- [27] T. Andersson, U. Stigh. The stress–elongation relation for an adhesive layer loaded in peel using Eq. uilibrium of energetic force. *Int. J. Sol Str.* 41 (2004) 413–434.
- [28] G. Ji, Z. Ouyang, G. Li, S. Ibekwe, Pang Su-Seng. Effect of adhesive thickenss on global and local Mode I interfacial fracture of bonded joints. *Inter J Sol Str.* 47(2010) 2445-2458.
- [29] G. Ji, Z. Ouyang, G. Li. Effects of bondline thickness on Mode-I nonlinear interfacial fracture of laminated composites: An experimental study. *Compos Part B.* 47(2013) 1–7.
- [30] BF. Sørensen, P. Kirkegaard. Determination of mixed mode cohesive laws. *Eng Fract Mech.* 73(2006) 2642–2661.
- [31] BF. Sørensen, TK. Jacobsen. Characterizing delamination of fibre composites by mixed mode cohesive laws. *Compos Sci Technol* 69 (2009) 445–456
- [32] A. de Morais, AB. Pereira. Application of the effective crack method to mode I and mode II interlaminar fracture of carbon/epoxy unidirectional laminates. *Compos Part A.* 38 (2007) 785–794.
- [33] D. Svensson, KS. Alfredsson, A. Biel, U. Stigh. Measurement of traction cohesive laws for interlaminar failure of CFRP *Compos Sci Technol* 100(2014) 53–62.
- [34] MM. Shokrieh, M. Salamat-talab, MM. Heidari-Rarani. Effect of initial crack length on the measured bridging law of unidirectional E-glass/epoxy double cantilever beam specimens. *Materials and Design* 55 (2014) 605–611
- [35] MM. Shokrieh, M. Salamat-talab, MM. Heidari-Rarani. Dependency of bridging traction of DCB composite specimen on interface fiber angle. *Theoretical and Applied Fracture Mechanics.* 90 (2017) 22-32
- [36] U. Stigh, K.S. Alfredsson, A. Biel, Measurement of cohesive laws and related problems, in: *IMECE 2009: Proceedings of the ASME International Mechanical Engineering Congress and Exposition.* 11 (2009) 293-298.
- [37] MFSF. De Moura, JPM. Gonçalves, AG. Magalhães. A straightforward method to obtain the cohesive laws of bonded joints under mode I loading. *International Journal of Adhesion and Adhesives.* 39 (2012) 54–9.
- [38] RMRP. Fernandes, JAG. Chousal, MFSF. de Moura, J. Xavier. Determination of cohesive laws of composite bonded joints under mode II loading. *Compos B Eng.* 52 (2013) 269–74.
- [39] N. Dourado, MFSF. de Moura, AB. de Morais, AB. Pereira. Bilinear approximations to the mode II delamination cohesive law using an inverse method. *Mech Mater* 49 (2012) 42–50.

-
- [40] A. Arrese, A. Boyano, J. de Gracia, F. Mujika. A novel procedure to determine the cohesive law in DCB tests. *Compos Sci. Technol.* 152 (2017) 76-84.
- [41] A. Arrese, N. Carbajal, G. Vargas, F. Mujika. A new method for determining mode II R-curve by the End-Notched flexure test. *Eng. Fract. Mech.* 77(2010) 77-20.
- [42] JR. Rice. A path independent integral and the approximate analysis of strain concentration by notches and cracks. *J Appl Mech* 35 (1968) 379–86.
- [43] Anderson TL. *Fracture Mechanics. Fundamentals and applications.* 2005
- [44] BF. Sorensen, TK. Jacobsen. Determination of traction cohesive laws by the J integral approach. *Engineering Fracture Mechanics* 70 (2003) 1841–1858
- [45] F. Mujika. On the effect of shear and local deformation in three point bending tests. *Polymer testing* 26 (2007) 869-77
- [46] JT. Oden, EA. Ripperger. *Mechanics of elastic structures.* 1981:460.
- [47] A. Arrese, F. Mujika. Influence of bending rotations on three and four-point bend end notched flexure test. *Engng Fract Mech* 75 (2008) 4234–46.
- [48] ABAQUS version 6.12: ABAQUS user’s manual, SIMULIA World Headquarters, 166 Valley Street, Providence, RI 02909, USA; 2012.